Acta Pharmaceutica Sinica B 2019;9(3):565–574

Chinese Pharmaceutical Association
Institute of Materia Medica, Chinese Academy of Medical Sciences

Acta Pharmaceutica Sinica B

www.elsevier.com/locate/apsb
www.sciencedirect.com

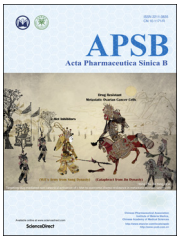

ORIGINAL ARTICLE

Safety and photochemotherapeutic application of poly(γ-glutamic acid)-based biopolymeric nanoparticle

Dongyoon Kim[a], Quoc-Viet Le[a], Young Bong Kim[b], Yu-Kyoung Oh[a,*]

[a]*College of Pharmacy and Research Institute of Pharmaceutical Sciences, Seoul National University, Seoul 08826, Republic of Korea*
[b]*Department of Biomedical Engineering, Konkuk University, Seoul 05029, Republic of Korea*

Received 1 October 2018; received in revised form 9 November 2018; accepted 15 November 2018

KEY WORDS

Safety;
Photochemotherapy;
Biopolymeric nanoparticle;
Poly(γ-glutamic acid);
Polymerized dopamine;
Paclitaxel

Abstract The safety of nanomaterials, a crucial consideration for clinical translation, is enhanced by using building blocks that are biologically nontoxic. Here, we used poly(γ-glutamic acid) (γ-PGA) and dopamine as building blocks of polymeric nanomaterials for carrying hydrophobic anticancer drugs. The introduction of phenylalanine onto γ-PGA enabled the resulting amphiphilic derivative of γ-PGA acid to self-assemble in the presence of the anticancer drug paclitaxel (PTX) to form PTX-encapsulated micelles. The surfaces of PTX-loaded micelles were then coated with polymerized dopamine (PDA). The PDA-coated, amphiphilic γ-PGA-based micelles (AM) carrying PTX (PDA/AM/P) exerted near-infrared-responsive photothermal effects. Near-infrared irradiation of cancer cells treated with PDA/AM/P nanoparticles produced a greater anticancer effect than that observed in other treatment groups, indicating a synergistic effect. Intravenous administration of PDA/AM/P completely ablated tumors and prevented their recurrence. Notably, the *in vivo* safety profile of PDA/AM/P nanoparticles allowed PTX to be delivered at a 3.6-fold higher dose than was possible with PTX solubilized in surfactant, and circumvented the side effects of the surfactant. These results support the multifunctional potential of PDA/AM for the delivery of various hydrophobic drugs and imaging dyes for safe translation of nanomaterials into the clinic.

*Corresponding author.
E-mail address: ohyk@snu.ac.kr (Yu-Kyoung Oh).

Peer review under responsibility of Institute of Materia Medica, Chinese Academy of Medical Sciences and Chinese Pharmaceutical Association.

https://doi.org/10.1016/j.apsb.2019.01.005

1. Introduction

Nanomaterials have been widely studied in the field of cancer therapy for use in producing formulations of poorly soluble drugs, diagnostic imaging, and tumor-directed delivery[1–4]. Several products are currently in clinical trials, and a few, including paclitaxel (PTX)-loaded polymeric micelles, are on the market for treatment of cancer patients[5]. Despite progress in the development of chemotherapeutics-loaded nanomaterials for cancer therapy, chemotherapy alone has limitations with respect to ablation of tumor tissues, in part reflecting dose-limiting consequences of adverse side effects. Moreover, the development of resistance against the drug often results in delayed tumor growth rather than tumor ablation[6].

Photothermal therapy has emerged as an alternative nanotechnology anticancer application for overcoming these limitations[7]. This technology is based on photothermal agents that absorb light and generate heat, thereby killing nearby cancer cells. By combining accumulation of photothermal agents in tumor tissue with near-infrared (NIR) irradiation of the tumor site with a laser, it is possible to achieve remotely controlled, spatiotemporally directed therapy[8]. However, laser-induced thermal ablation suffers from incomplete eradication of cancer cells owing to heterogeneous heat distribution in tumor tissue. The limited intensity of light in deeper tissues also leads to an insufficient thermal-killing effect as the light passes through the tumor tissue[9].

Photochemotherapy—combining chemotherapy and photothermal therapy—produces complementary effects that transcend the limitations of each therapy alone, and thus has been studied as a promising strategy for treating cancer. Improved therapeutic efficacy of photochemotherapy has been reported using various nanomaterials incorporating photoresponsive components. These applications include tungsten disulfide quantum dots on doxorubicin-loaded mesoporous silica nanoparticles[10]. bismuth selenide nanoparticles[11], and graphene-based nanosheets loaded with anticancer chemotherapeutics[12].

However, most such studies have used nanomaterials that cannot be translated to the clinic owing to their lack of biocompatibility, underscoring the importance of developing safe and effective nanomaterials that retain the ability to confer effective photochemotherapy. Ultimately, enhancing the safety of such nanomedicines requires that their nanomaterial building blocks be biologically nontoxic.

In this study, we focused on the use of nontoxic natural components for the design of safe nanomaterials. Poly(γ-glutamic acid) (γ-PGA) is a natural biopolymer produced by bacteria, especially *Bacillus* species. Because of its high solubility, biodegradability and low toxicity, γ-PGA has been used in diverse biomedical applications, including as a drug-delivery system, and as a material for tissue engineering and biological adhesives[13].

Polymerized dopamine (PDA) is a biopolymer inspired from mussel. PDA is a polymerized form of dopamine, which is one of endogenous neurotransmitters secreted from central nervous system. The lack of dopamine secretion is known to be related to Parkinson's disease[14]. In the presence of oxygen in basic condition, dopamine is oxidized into dopamine-quinone and 5,6-dihydroxyindole through intramolecular cyclization. Dopamine-quinone and 5,6-dihydroxyindole then act as key building block monomers of polymerization, resulting in PDA[15].

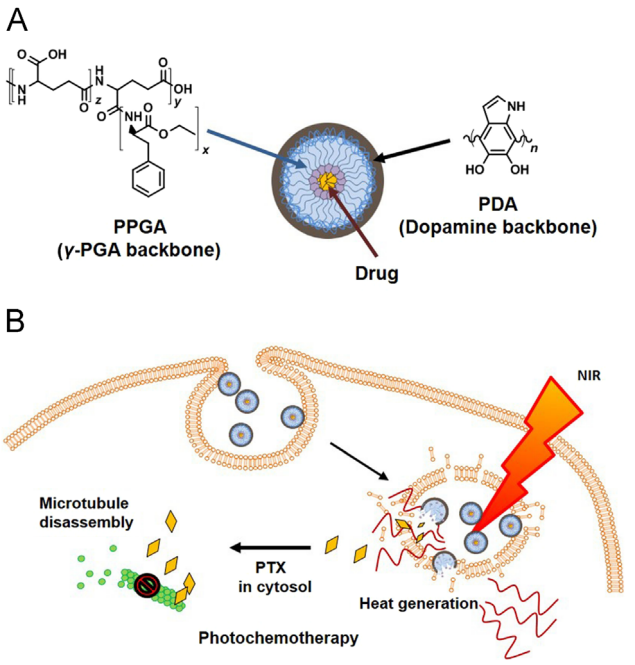

Figure 1 Illustration of PDA/AM/P nanoparticle structure and the mechanism of photochemotherapy. (A) A schematic illustration depicting the construction of PDA/AM/P containing PTX as a hydrophobic drug in their core. (B) Application of PDA/AM/P nanoparticles for induction of synergistic anticancer effects by photochemotherapy.

The mechanism by which PDA can exert photothermal property is due to its dense pi conjugation systems of *sp*2 hybridized carbons. In PDA, the absorption of light energy leads to the oscillation of electrons, and the surface plasmon resonance release the vibration energy as heat. The molar extinction coefficient of PDA at 808 nm is reported[16] to be 7.3×10^8 $M^{-1} \cdot cm^{-1}$.

The photothermal feature of PDA nanomaterial has been applied to anticancer phototherapy. PDA alone has been used to induce local hyperthermia upon irradiation with NIR[17]. In some studies, PDA has been used to coat the surfaces of gold nanorods[18], graphene oxide nanosheets[19], and iron oxide nanoparticles[20]. However, in these studies, the core nanomaterials coated with PDA have suffered from the lack of biodegradable properties.

In this study, we used an amphiphilic phenylalanine derivative of γ-PGA (PPGA) to form biopolymeric self-assembled micelles loaded with the hydrophobic anticancer drug, PTX. To confer photothermal property to the PTX-loaded nanoparticles, we used PDA as a surface coating material. Here, we report the safety and photochemotherapeutic efficacy of the resulting γ-PGA- and dopamine-based, PTX-carrying PDA/AM/P nanoparticles (Fig. 1).

2. Materials and methods

2.1. *Synthesis of PPGA*

PPGA was synthesized through amide coupling between γ-PGA (50 kDa; BioLeaders, Daejeon, Republic of Korea) and

phenylalanine ethylester (Sigma, St. Louis, MO, USA) as described previously[21]. In brief, 10 g of γ-PGA was dissolved in 1 L of 0.3 mol/L $NaHCO_3$ solution, to which was added 15 g of 1-(3-dimethylaminopropyl)-3-ethylcarbodiimide hydrochloride (EDC; Tokyo Chemical Industry Co., Ltd., Tokyo, Japan), followed by stirring for 30 min on ice. Next, 18 g of phenylalanine ethylester was added, and the solution was stirred for 24 h at 37 °C. The resulting PPGA was purified by dialysis against triple-distilled water (TDW) for 24 h, and then against methanol for 24 h using a Spectra/Pore dialysis membrane (molecular weight cut-off, 3 kDa; Spectrum Labs, Rancho Dominguez, CA, USA). The dialysate was lyophilized to obtain PPGA in powdered form. The structure of PPGA was depicted in Fig. 1 and confirmed by ^{1}H NMR spectroscopy[22].

2.2. Preparation of PDA-coated nanoparticles

PTX (Sigma) was loaded into PPGA-based, self-assembled micelles using a thin-film hydration method[23]. Initially, 5 mg of PPGA and 100 μg of PTX were mixed in 1 mL of methanol, and the organic solvents were removed using a rotary evaporator (CCA-1110; Tokyo Rikakikai, Tokyo, Japan). After evaporation was complete (4 h), the resulting thin films were hydrated with 1 mL of tris(hydroxymethyl)aminomethane buffer (10 mmol/L Tris pH 9.0), vortexed, and then sonicated for 1 h. Unencapsulated PTX was removed by centrifugation at 10,000 × *g* for 3 min. The resulting PTX-loaded amphiphilic PPGA self-assembled micelles (AM/P) were then coated with PDA, mixed with the same volume of PDA solution (20 mg/mL) in 10 mmol/L Tris buffer, and incubated at room temperature for 24 h, forming PDA-coated AM/P (PDA/AM/P) nanoparticles. The nanoparticles were purified by removing unpolymerized PDA using a PD-10 column (GE Healthcare, Buckinghamshire, UK).

2.3. Quantification of PTX in nanoparticles

The amount of PTX encapsulated in AM/P was quantified by high-performance liquid chromatography (HPLC) on a Hewlett Packard model 1100 system (Hewlett Packard, Palo Alto, CA, USA). Lyophilized nanoparticles were dissolved in 1 mL of MeOH and injected onto a reverse-phase C18 HPLC column (Nucleosil 100-5 C18; Macherey-Nagel, Düren, Germany) at 20 °C in a volume of 20 μL. The columns was eluted using a mobile phase of acetonitrile:water (48:52, *v/v*) and a flow rate of 1 mL/min. PTX was measured by UV detection at 227 nm, and its concentration was determined by reference to calibration curves . For determination of PTX release profile, 1 mL of PTX-loaded nanoparticles in a dialysis bag (molecular weight cut-off, 3.5 kDa; Spectrum Labs) was incubated in 40 mL PBS with 0.1% (*w/v*) Tween 80 (Sigma) at 37 °C. At various time points, 1 mL of the samples was freeze dried, reconstituted in 200 μL of methanol, and analyzed by HPLC using a C18 column.

2.4. Size, zeta potential, and morphology measurement of nanoparticles

The size of AM/P and PDA/AM/P nanoparticles were measured by dynamic light scattering (DLS) using a He-Ne laser (10 mW). Zeta potentials of nanoparticles were measured by laser Doppler microelectrophoresis at an angle of 22° using an ELSZ-1000 instrument (Otsuka Electronics Co., Osaka, Japan). The morphology of AM/P and PDA/AM/P nanoparticles was examined by scanning electron microscopy (SEM). SEM samples were prepared by placing PDA/AM/P nanoparticles on a 12-mm diameter copper grid (FESEM finder grid; Ted Pella Inc., Redding, CA, USA), and SEM images were obtained using a Field-Emission SEM/FIB (focused ion beam) system (Carl Zeiss Inc., Thornwood, NY, USA). Morphology of the nanoparticles was also examined by transmission electron microscopy (TEM, Talos L120C, Thermo Fisher Scientific, Inc, Waltham, MA, USA) after negative staining.

2.5. Measurement of photothermal effects

Photothermal effects of nanoparticles were characterized by measuring changes in temperature upon NIR irradiation. Suspensions of nanoparticles in TDW were irradiated with an 808 nm NIR diode laser at an output power of 1.5 W (BWT Beijing LTD, Beijing, China) for 1 min and then cooled for 4 min. Temperature changes of the samples were measured using an FLIR T420 IR thermal imaging system (FLIR System Inc., Danderyd, Sweden).

2.6. In vitro assessment of anticancer effects

In vitro anticancer effects were determined by measuring the viability of NIR-irradiated, nanoparticle-treated cells. CT-26 murine colon carcinoma cells (American Type Culture Collection, Manassas, VA, USA) were cultured in RPMI-1640 media (Welgene, Daegu, Republic of Korea) supplemented with 10% fetal bovine serum, 100 units/mL penicillin and 100 μg/mL streptomycin. CT-26 cells were seeded onto 48-well plates (SPL Life Sciences, Pocheon, Republic of Korea) at a density of 1×10^5 cells/well. The next day, cells were treated for 24 h with free PTX in dimethyl sulfoxide (DMSO) or PDA/AM/P, each at a PTX concentration of 10 μg/mL. After washing cells with phosphate-buffered saline (PBS), cell pellets were irradiated with an 808 nm NIR laser at a power of 1.5 W, and the temperatures of samples were measured with an FLIR T420 real-time IR thermal imaging system. After irradiation, cells were seeded onto 96-well plates (SPL Life Sciences) and incubated for 24 h. The viability of the cells was then quantified with a Cell Counting Kit 8 (Dojindo, Molecular Technologies, Inc., Rockville, MD, USA). Calcein AM staining (Molecular Probes, Eugene, OR, USA) was also used to visualize live cells.

2.7. In vivo safety

Acute *in vivo* toxicity was evaluated by intravenously injecting 15 to 20-week-old BALB/c mice (OrientBio, Seongnam, Korea) with different doses of PTX (10 to 150 mg/kg) in 5% glucose solution. The survival rate was recorded 1 day post dosing ($n = 5$ mice/group). In some experiments, mice were treated with a commercial PTX formulation solubilized with Cremophor EL (polyethoxylated castor oil; Sigma). The Cremophor EL-based PTX formulation was prepared by solubilizing PTX at a concentration of 6 mg/mL in a mixture of Cremophor EL and dehydrated alcohol (50:50, *v/v*). The median 50% lethal dose (LD_{50}) was calculated according to a previous report[24].

Blood and serum samples were analyzed for hematological and biochemical parameters by the Neodin VET Diagnostics Institute (Seoul, Republic of Korea). Hematological parameters included

white blood cell (WBC), red blood cell (RBC), platelet, neutrophil, lymphocyte, monocyte and eosinophil counts; hematocrit (Hct); mean corpuscular volume (MCV); hemoglobin (Hb); mean corpuscular Hb (MCH); and mean corpuscular Hb concentration (MCHC). Biochemical parameters included blood urea nitrogen (BUN), creatinine, aspartate transaminase (AST), alanine aminotransferase (ALT), and bilirubin.

For hemolysis assays, RBCs (2×10^4 cells/mL) from each treatment group were suspended in PBS and incubated for 2 h at 37 °C; for PTX-containing groups, the PTX concentration was 50 mg/kg. After incubation, samples were centrifuged at $16{,}000 \times g$ for 60 min, and RBC lysis was determined by assessing absorbance of supernatants at 450 nm using a spectrophotometer (Tecan, Männedorf, Switzerland).

2.8. *In vivo study of photochemotherapeutic efficacy*

The *in vivo* photochemotherapeutic efficacy of PDA/AM/P nanoparticles was evaluated using a CT-26 tumor-bearing mouse model, prepared by subcutaneously inoculating BALB/c mice (OrientBio) with 5×10^5 CT-26 cells. When tumors reached a volume of $\sim 100\,mm^3$, 4 mg/kg of PTX in free form with Cremophor EL or in nanoparticle formulations was intravenously administered ($n = 5$ mice/group). One day post dosing, tumors were irradiated with an 808 nm NIR laser at a power of 1.5 W for 10 min. Temperature and thermal images of the irradiated tumor site were measured with an FLIR T420 real-time IR thermal imaging system. Tumor dimensions were measured with calipers beginning 1 day after irradiation, and tumor volume was calculated as described previously[25].

For immunohistochemical detection of proliferating cells, extracted tumors were fixed, sectioned, and stained with an antibody against anti-proliferating cell nuclear antigen (PCNA; Thermo-Fisher Scientific, Waltham, MA, USA). Apoptosis in tumor sections was assessed by terminal deoxynucleotidyl transferase dUTP nick-end labeling (TUNEL) assay (Millipore Corp., Billerica, MA, USA). Stained tumor sections were examined using an Eclipse TE2000-S microscope (Nikon, Tokyo, Japan), and areas of proliferating and apoptotic cells were calculated using Image-Pro Plus Version 6.0 image analysis software (Media Cybernetics, Inc., Rockville, MD, USA).

2.9. *Statistics*

The statistical significance of differences among groups was analyzed by analysis of variance (ANOVA) with a post hoc Student-Newman-Keuls test using SigmaStat software (Systat Software, San Jose, CA, USA). A *P*-value less than 0.05 was considered statistically significant.

3. Results

3.1. *Physicochemical properties of nanoparticles*

PTX was encapsulated during the AM self-assembly process, and then the surfaces of AM/P were coated with PDA (Supporting Information Fig. S1). A ^{1}H NMR spectrometric analysis showed that the grafting ratio of phenyl groups in the γ-PGA polymer backbone was 25.9% (Supporting Information Fig. S2B). The self-assembled size of plain amphiphilic PPGA-based micelle (AM) was slightly larger than that of PTX-loaded AM (AM/P). Surface coating of AM/P with PDA (PDA/AM/P) did not significantly affect nanoparticle size (Fig. 2A) but did alter zeta potentials (Fig. 2C). Zeta potential values were highly negative for both plain AM and AM/P nanoparticles. After PDA coating, PDA/AM and PDA/AM/P nanoparticles showed significantly decreased potential values of –22.68 and –16.57 mV, respectively (Fig. 2C). SEM revealed that both AM/P and PDA/AM/P were spherical (Fig. 2D). The surfaces of PDA/AM/P look slightly rough compared to the smooth surfaces of AM/P. Consistent with SEM, TEM showed the spherical morphologies for both AM/P and PDA/AM/P (Fig. 2E). Notably, the enlarged TEM figure (Fig. 2E, inset) showed a rim-like structure in PDA/AM/P.

Encapsulation of PTX in AM increased its dispersity in PBS. Free PTX (50 μg/mL) formed aggregates owing to its limited solubility in PBS, whereas PTX in all AM and PDA-coated AM nanoparticles was stably dispersed in PBS (Fig. 2F). The release of PTX from nanoparticles was slightly slower after surface coating with PDA. PTX was gradually released from nanoparticles, and the release amount of PTX from AM/P and PDA/AM/P were 68.7% and 58.8%, respectively, after 3 days of incubation (Fig. 2G).

The presence of PDA on AM/P nanoparticles conferred photo-responsive properties upon NIR irradiation. PDA/AM and PDA/AM/P showed notably high absorbance at 808 nm (Supporting Information Fig. S3). This NIR-responsive photothermal property was observed in PDA/AM and PDA/AM/P nanoparticles, but not in AM or AM/P nanoparticles (Fig. 2H). The temperature of PDA/AM/P nanoparticles increased rapidly up to 70 °C upon NIR irradiation and decreased to room temperature following cessation of NIR irradiation. The temperature increase was dependent on the concentrations of PDA/AM/P (Supporting Information Fig. S4).

3.2. *In vivo safety of PDA/AM/P nanoparticles*

Hemolysis assays showed greater hemocompatibility of PDA/AM/P formulations compared with free PTX in Cremophor. At a dose of 50 mg/kg, the hemolytic activity of PTX in Cremophor was 80.6% (Fig. 2I and J). In dramatic contrast, PDA/AM/P nanoparticles showed no interaction with RBCs, indicating that this nanoformulation of PTX is hemocompatible.

PDA/AM/P and AM/P nanoparticles showed higher safety profiles compared with PTX in Cremophor (Fig. 3A). A PTX dose-escalation study showed that the survival of mice treated with free PTX in Cremophor started to decrease at a dose of 60 mg/kg. Complete mortality was observed at doses higher than 80 mg/kg. In contrast, neither AM/P nor PDA/AM/P nanoparticles caused any mortality at a dose of PTX in Cremophor that was lethal. The calculated LD_{50} values for both AM/P and PDA/AM/P nanoparticles were greater than 150 mg/kg (Table 1).

Unlike Cre/P, PDA/AM/P did not induce notable changes in biochemical and hematological parameters (Fig. 3). Compared to untreated group, Cre/P-treated group induced 30.1-, 2.5-, and 1.6-fold higher levels of ALT (Fig. 3B), AST (Fig. 3C), and BUN (Fig. 3D), respectively. Hematological assay revealed that Cre/P treatment significantly increased neutrophils with decrease of lymphocytes (Fig. 3E). The ratio of neutrophil to lymphocyte, was

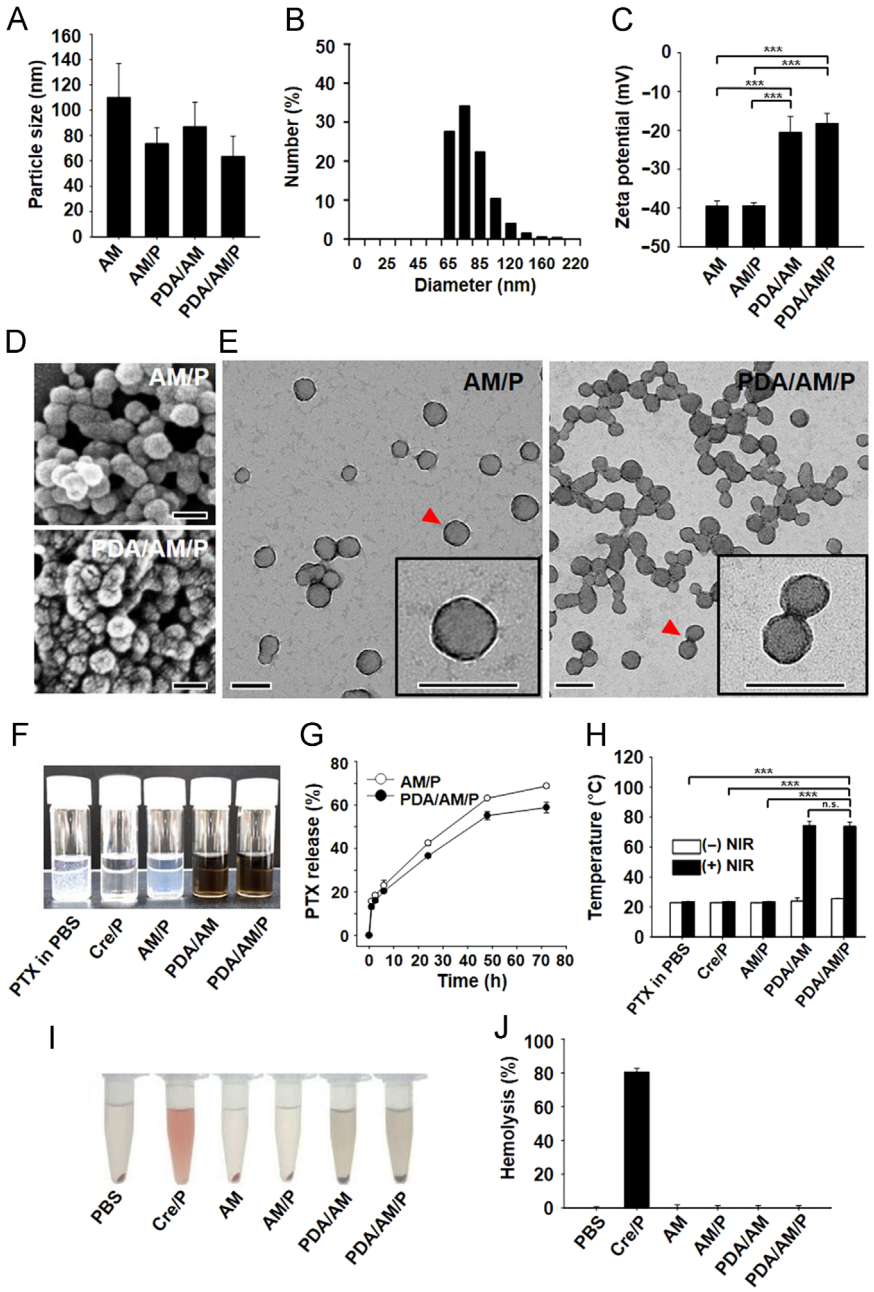

Figure 2 Characterization and hemocompatibility of PDA/AM/P nanoparticle. (A) The size of various nanoparticles and (B) the size distribution of PDA/AM/P were measured using DLS. (C) Zeta potential of nanoparticles was measured by laser Doppler microelectrophoresis. (D) and (E) The morphology of PDA/AM/P was observed by SEM and TEM (Scale bar = 100 nm). The red arrowed particles were enlarged and presented as inset figures. (F) Aqueous dispersion stability of PTX in free form or in nanoparticle formulations was evaluated in PBS at a PTX concentration of 50 μg/mL. (G) Release of PTX from nanoparticles was measured by HPLC ($n = 3$). (H) Photothermal effects of PDA-coated nanoparticles were assessed by measuring temperature upon repeated irradiation with 808 nm laser light at a concentration of 2.5 mg/mL. Hemocompatibility of each formulation was visualized by adding each sample to RBC (I) and quantified by hemolysis assay (J).

3.3-fold higher in Cre/P-treated group as compared to untreated group (Fig. 3F). After PDA/AM/P-treatment, the ratio of neurophil to lymphocyte was 1.4-fold higher than untreated group.

3.3. *In vitro anticancer effects of PDA/AM/P nanoparticles*

The chemotherapeutic anticancer effects of PDA/AM/P nanoparticles were enhanced by NIR irradiation. Cells treated with free PTX or AM/P nanoparticles showed no increase in temperature, regardless of NIR irradiation. However, upon NIR irradiation, the temperature of cells treated with PDA/AM or PDA/AM/P nanoparticles increased to greater than 44 °C (Fig. 4A and B), an increase that paralleled the enhanced anticancer effect. In the absence of NIR irradiation, the viability of cancer cells was $37.1 \pm 1.0\%$ in the group treated with PDA/AM/P nanoparticles. However, upon NIR irradiation, the viability of PDA/AM/P-treated CT26 cancer cells was reduced to $4.7 \pm 0.2\%$ (Fig. 4C).

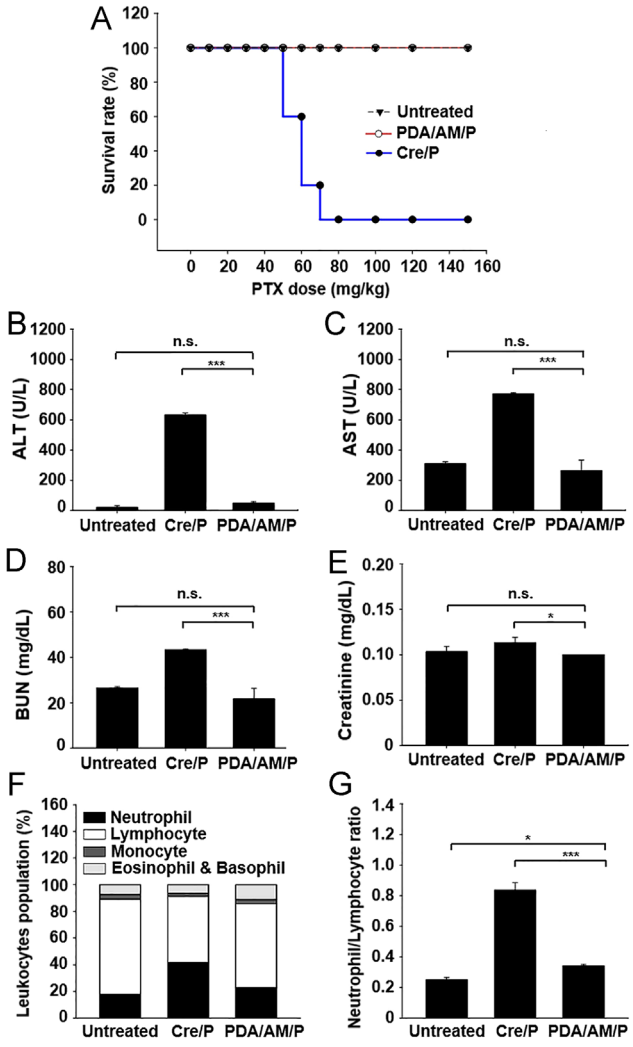

Figure 3 *In vivo* safety of PTX formulations. (A) Mice were injected with Cremophor-, AM-, or PDA/AM-based PTX formulations at various doses, and the safety of each formulation was evaluated by monitoring survival rates ($n=5$). One day after dosing with various formulations of PTX, blood was extracted and analyzed for the biochemical parameters, ALT (B), AST (C), BUN (D), and creatinine (E). One day after dosing with various formulations of PTX, leukocyte populations (F) and the ratios of neutrophil to lymphocyte (G) were assessed. $^{*}P<0.05$, $^{***}P<0.001$.

Consistent with quantitative assessments of cell viability, live-cell fluorescence staining showed that cells treated with PDA/AM/P nanoparticles exhibited the lowest percentage of viable cells among treatment groups following NIR irradiation (Fig. 4D).

3.4. *In vivo photochemotherapeutic effect of PDA/AM/P nanoparticles*

In CT26 tumor-bearing mice, NIR irradiation of tumor tissues in mice treated with PDA/AM/P nanoparticles increased tissue temperature (Fig. 5A and B) and ablated the growth of tumors (Fig. 5D). Upon NIR irradiation, the temperature of tumor tissues in groups treated with Cremophor-based PTX, AM, or AM/P was 37 °C. However, in groups treated with PDA/AM or PDA/AM/P nanoparticles, the temperature of tumor tissues increased to 50 °C upon NIR irradiation (Fig. 6B). Although both PDA/AM and PDA/AM/P nanoparticles exerted similar photothermal effects, only PDA/AM/P nanoparticles exerted a tumor-ablating effect (Fig. 5C–E). Immunohistochemical staining of tumor tissues showed that mice treated with PDA/AM/P nanoparticles had the lowest population of proliferating cells (Fig. 6A and C) and the highest percentage of apoptotic cells (Fig. 6B and D) of all treatment groups.

4. Discussion

Here, we demonstrated that hydrophobic drugs, such as PTX, can be encapsulated in self-assembled AM, and surface-coated with PDA to provide NIR-responsive photothermal and chemotherapeutic anticancer effects. Moreover, we showed that the use of biopolymeric AM for encapsulation of hydrophobic drug and PDA coating provides a safe and biocompatible nanotechnology platform.

The self-assembly of AM into micelles was achieved by introducing a phenylalanine moiety to create a hydrophobic core, into which was loaded PTX, one of a number of hydrophobic

anticancer drugs. Notably, we observed that the size of AM decreased after PTX loading and PDA surface coating. The reduction of nanoparticle size upon PTX loading may be explained by the hydrophobic interactions between PTX and phenylalanine moieties of AM. Consistent with our observation, a previous study showed a reduction of mean particle size of pegylated lipid-based micelles after loading meso-tetraphenylporphine into the hydrophobic micellar core[26].

The mechanisms by which PDA coats the surface of AM/P nanoparticles will require further investigation. However, several studies have reported the phenomena of PDA coating of micelles of various solid surfaces, such as cell adhesion membranes[27], silica[28] and gold nanoparticles[29], for the introduction of surface modifications through noncovalent interactions.

It has been reported that PDA coating mechanism mainly depends on pi–pi interaction, charge interaction or hydrogen bonding[11]. In this study, driving force for surface coating of AM/P with PDA could be mainly explained by the hydrogen bonding between oxygen in carboxylic groups of AM and hydrogen in primary or secondary amine groups of PDA. Moreover, the high density of catechol groups on PDA surface might contribute to the hydrogen bonding between catechol groups and hydrogen in the amide bond of AM. During the PDA surface coating process of the AM/P nanoparticles, the tight hydrogen bonding interaction between PDA and AM/P may result in condensation of the core, decreasing the overall particle size slightly. The reduction of nanoparticle sizes due to noncovalent interactions has been previously reported[30]. In the study, the sizes of positively charged chitosan-modified liposomes were shown to decrease after surface coating with negatively charged alginate *via* electrostatic interaction[30].

Compared with other PTX formulations, PDA/AM/P nanoparticles provided the greatest *in vitro* and *in vivo* anticancer effects upon NIR irradiation. This enhanced activity likely reflects the synergistic anticancer activity attributable to the combination of NIR-responsive photothermal and PTX-mediated anticancer effects. Since the mechanism underlying PTX effects is known to involve binding to the cytoskeleton[31], the prediction is that PTX is liberated into the cytoplasm of cells. Photothermal stimulation may operate through dual modes to contribute to the anticancer effect of PDA/AM/T nanoparticles. First, the increase in temperature induced by the external PDA coating layer increased tumor cell apoptosis, as revealed by TUNNEL assays (Fig. 6D). The second mechanism is the photochemical liberation of PTX from endosomes into the cytoplasm. Such photochemical liberation of chemotherapeutic drugs into the cytoplasm has been previously reported[17]. Possible mechanisms of action of PDA/AM/P nanoparticles are illustrated in Fig. 1B.

In addition to the observed synergistic anticancer effects, another advantage of PDA/AM/P nanoparticles is their biocompatibility. Numerous studies have reported photothermal therapy and chemotherapy using various materials. However, most such studies used inorganic metals, such as bismuth[32], gold[33], silver[34] or copper[35]—approaches that cannot be readily translated into the clinic owing to regulatory concerns regarding safety issues. In the current study, we used AM for surface coating with PDA. Since AM is derived from the natural biopolymer PGA, a bacterial component used to avoid recognition by the immune system, it is biodegradable in the body. Survival data from dose-escalation studies in mice performed here support the safety of PDA/AM/P nanoparticles.

Table 1 Tolerable and lethal doses of PTX in various formulations.

Group	MTD (mg/kg)	Lethal dose (mg/kg)	LD_{50} (mg/kg)
Cre/P	50	80	43
AM/P	>150	>150	>150
PDA/AM/P	>150	>150	>150

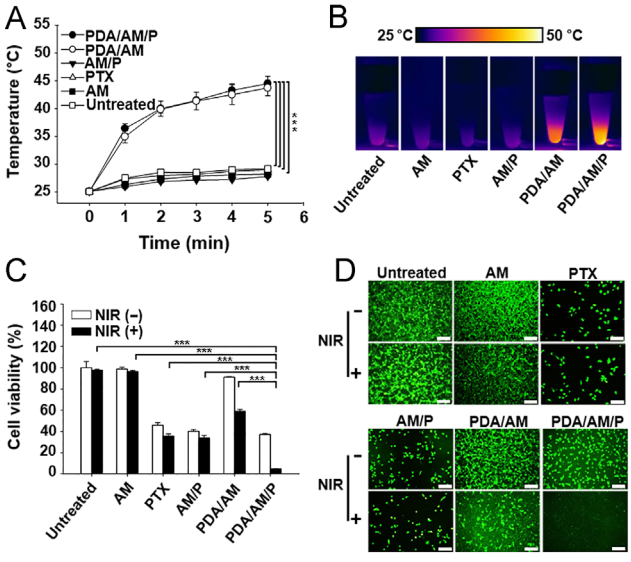

Figure 4 *In vitro* synergistic effects of chemotherapy and photothermal therapy. CT-26 cells were treated with PDA/AM/P nanoparticles at a PTX concentration of 10 μg/mL and, after incubating for 24 h, were irradiated with a NIR laser for 5 min. Temperature (A) was measured during irradiation, and thermal images (B) were measured after 5 min of irradiation. Irradiated and non-irradiated cells were incubated for an additional 24 h, after which viability was assessed (C) and live-cell staining was performed (D) (Scale bar = 100 μm).

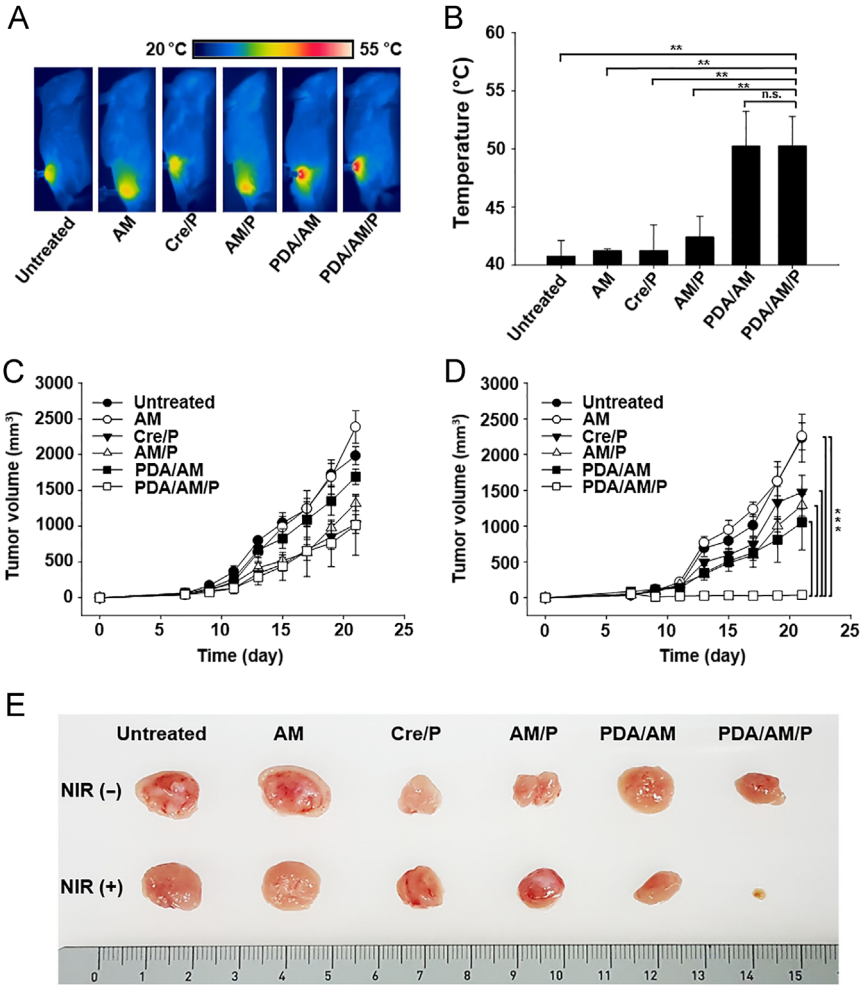

Figure 5 *In vivo* synergistic effect of PTX and NIR irradiation. CT-26 tumor-bearing mice were injected intravenously with PTX in various formulations. One day after dosing, tumors were irradiated with an 808 nm NIR laser for 10 min ($n=5$). Thermal images (A) and temperature (B) of irradiated tumor sites were measured during irradiation. *In vivo* anticancer efficacy was evaluated by measuring tumor size without NIR irradiation (C) and with NIR irradiation (D). (E) Representative photographs of tumor volumes are presented (Scale unit: cm).

PDA and melanin have been known to be degraded by hydrogen peroxide generated by reduced nicotinamide adenine dinucleotide phosphate (NADPH) oxidases abundant in phagocytes and various tissues[14]. A recent study reported that PDA was indeed degraded by hydrogen peroxide within 24 h[16]. Although there is little report on the *in vivo* degradation of PDA *per se*, one study reported the erosion and degradation of melanin after implantation[36]. Since melanin and PDA are structurally similar and susceptible to hydrogen peroxide-mediated degradation, there exists a possibility that PDA may undergo biodegradation pathways similar to melanin *in vivo*. However, more direct studies on the *in vivo* degradation mechanism of PDA need to be done in the near future.

The encapsulation of hydrophobic drugs such as PTX can avoid the use of harmful surfactants such as Cremophor, which is known to induce toxic inflammatory reactions[37,38]. The improved safety of PPGA-based PTX formulations compared with the conventional clinical formulation could be explained by their enhanced hemocompatibility and reduced systemic toxicity. We observed that Cre/P treatment elevated the ratio of neutrophil to lymphocyte. The ratio of neutrophil to lymphocyte has been used as an indicator of systemic inflammation[39,40]. The normal range of the neutrophil to lymphocyte ratio has been reported to be 0.2 and 0.3[41]. Although the ratio of neutrophil to lymphocyte in PDA/AM/P-treated group was slightly increased to untreated group in this study, it was 0.34 near the normal range of the ratio. ALT and AST are biochemical parameters for assessing hepatic toxicity[42]. BUN and creatinine have been used as markers of renal toxicity[43]. Cre/P treatment exerted significant hepatic and renal toxicity evidenced by the alterations of various parameters. No significant changes of biochemical parameters after PDA/AM/P treatment support that PDA/AM/P did not affect the hepatic and renal functions. The lack of hematological and organ toxicity after administration of PDA/AM/P might be attributed to the biocompatibility of glutamic acid and dopamine, which might be produced upon degradation of PDA/AM/P in the body.

Although we used PTX as a model hydrophobic drug in this study, the concept of self-assembled AM can be extended to

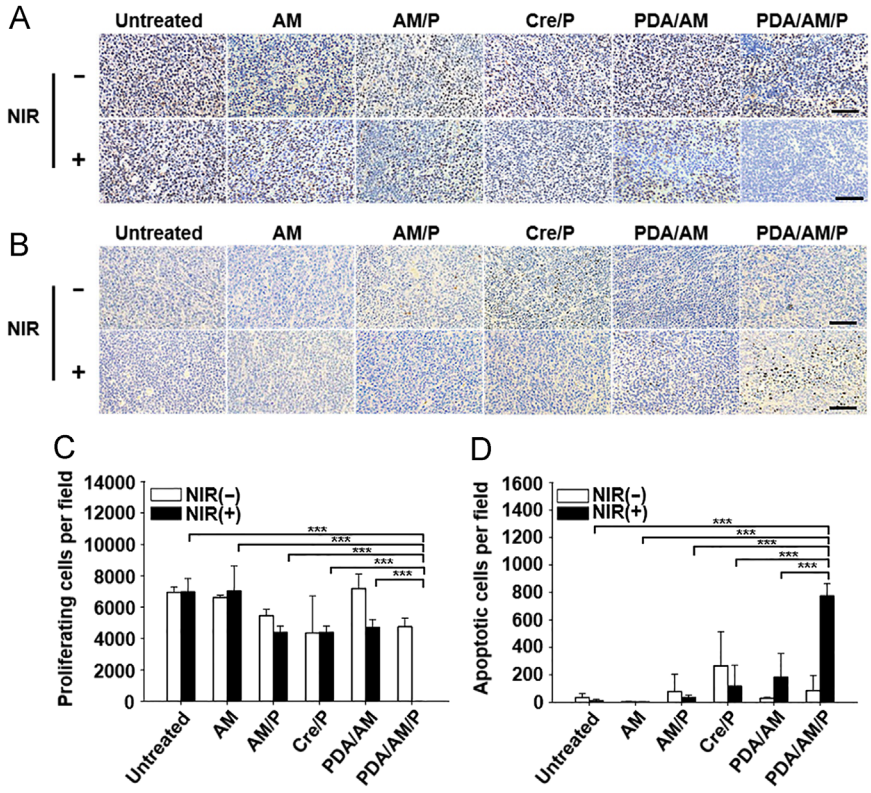

Figure 6 Immunohistochemistry of tumor after chemo and photothermal combination therapy. Tumor tissues were extracted and stained for PCNA and TUNEL assay. The proliferating cells in the tumor tissue were visualized by PCNA staining (A) and apoptotic cells were visualized by TUNEL staining (B) (Scale bar = 100 μm). The proliferating cells per field (C) and apoptotic cells per field (D) were quantitatively analyzed by image analysis software. $^{***}P < 0.001$.

encapsulation of other hydrophobic components, such as hydrophobic dyes and radiopharmaceuticals for imaging purposes. Moreover, surface coating with NIR-responsive PDA could ultimately be used for the design of multifunctional nanoparticles that provide imaging, chemical, and photothermal effects.

5. Conclusions

We demonstrated that biopolymeric PGA-derived AM can self-assemble and encapsulate PTX into its hydrophobic core. Surface coating with PDA conferred photothermal properties on PDA/AM/P, allowing these nanoparticles to exert chemotherapeutic anticancer effects. The safety profile and hemocompatibility supports the conclusion that PDA/AM/P nanoparticles may be used for a broad spectrum of biomedical applications, including imaging, and serve as a multifunctional nanoplatform.

Acknowledgments

This research was supported by grants from the Ministry of Science and ICT, Republic of Korea (NRF-2018R1A2A1A05019203 and NRF-2018R1A5A2024425) and from the Korean Health Technology R&D Project (Nos. HI15C2842 and HI18C2177), Ministry of Health & Welfare, Republic of Korea.

Appendix A. Supporting information

Supplementary data associated with this article can be found in the online version at https://doi.org/10.1016/j.apsb.2019.01.005.

References

1. Shi J, Kantoff PW, Wooster R, Farokhzad OC. Cancer nanomedicine: progress, challenges and opportunities. *Nat Rev Cancer* 2017;**17**:20–36.
2. Adiseshaiah PP, Crist RM, Hook SS, McNeil SE. Nanomedicine strategies to overcome the pathophysiological barriers of pancreatic cancer. *Nat Rev Clin Oncol* 2016;**13**:750–65.
3. Chowdhury P, Nagesh PK, Khan S, Hafeez BB, Chauhan SC, Jaggi M, et al. Development of polyvinylpyrrolidone/paclitaxel self-assemblies for breast cancer. *Acta Pharm Sin B* 2018;**8**:602–14.
4. Zhao J, Chen J, Ma S, Liu Q, Huang L, Chen X, et al. Recent developments in multimodality fluorescence imaging probes. *Acta Pharm Sin B* 2018;**8**:320–38.
5. Anselmo AC, S. Mitragotri S. Nanoparticles in the clinic. *Bioeng Transl Med* 2016;**1**:10–29.

6. Bumbaca B, Li W. Taxane resistance in castration-resistant prostate cancer: mechanisms and therapeutic strategies. *Acta Pharm Sin B* 2018;**8**:518–29.
7. Chu KF, Dupuy DE. Thermal ablation of tumours: biological mechanisms and advances in therapy. *Nat Rev Cancer* 2014;**14**:199–208.
8. Tang X, Tan L, Shi K, Peng J, Xiao Y, Li W, et al. Gold nanorods together with HSP inhibitor-VER-155008 micelles for colon cancer mild-temperature photothermal therapy. *Acta Pharm Sin B* 2018;**8**:587–601.
9. Hashida Y, Tanaka H, Zhou S, Kawakami S, Yamashita F, Murakami T, et al. Photothermal ablation of tumor cells using a single-walled carbon nanotube–peptide composite. *J Control Release* 2014;**173**:59–66.
10. Lei Q, Wang SB, Hu JJ, Lin YX, Zhu CH, Rong L, et al. Stimuli-responsive "Cluster Bomb" for programmed tumor therapy. *ACS Nano* 2017;**11**:7201–14.
11. Li Z, Liu J, Hu Y, Howard KA, Li Z, Fan X, et al. Multimodal imaging-guided antitumor photothermal therapy and drug delivery using bismuth selenide spherical sponge. *ACS Nano* 2016;**10**:9646–58.
12. Su YL, Yu TW, Chiang WH, Chiu HC, Chang CH, Chiang CS, et al. Hierarchically targeted and penetrated delivery of drugs to tumors by size-changeable graphene quantum dot nanoaircrafts for photolytic therapy. *Adv Funct Mater* 2017;**27**:170056.
13. Ogunleye A, Bhat A, Irorere VU, Hill D, Williams C, Radecka I. Poly-γ-glutamic acid: production, properties and applications. *Microbiology* 2015;**61**:1–17.
14. Liu X, Cao J, Li H, Li J, Jin Q, Ren K, et al. Mussel-inspired polydopamine: a biocompatible and ultrastable coating for nanoparticles *in vivo*. *ACS Nano* 2013;**7**:9384–95.
15. Ryu JH, Messersmith PB, Lee H. Polydopamine surface chemistry: a decade of discovery. *ACS Appl Mater Interfaces* 2018;**10**:7523–40.
16. Liu Y, Ai K, Liu J, Deng M, He Y, Lu L. Dopamine-melanin colloidal nanospheres: an efficient near-infrared photothermal therapeutic agent for *in vivo* cancer therapy. *Adv Mater* 2013;**25**:1353–9.
17. Shim G, Ko S, Kim D, Le QV, Park GT, Lee J, et al. Light-switchable systems for remotely controlled drug delivery. *J Control Release* 2017;**267**:67–79.
18. Zhang L, Su H, Cai J, Cheng D, Ma Y, Zhang J, et al. A multifunctional platform for tumor angiogenesis-targeted chemo-thermal therapy using polydopamine-coated gold nanorods. *ACS Nano* 2016;**10**:10404–17.
19. Kim H, Kim DW, Vasagar V, Ha H, Nazarenko S, Ellison CJ. Polydopamine-graphene oxide flame retardant nanocoatings applied *via* an aqueous liquid crystalline scaffold. *Adv Funct Mater* 2018;**28**:1803172.
20. Yu S, Li G, Liu R, Ma D, Xue W. Dendritic Fe3O4@ poly(dopamine) @PAMAM nanocomposite as controllable NO-releasing material: a synergistic photothermal and NO antibacterial study. *Adv Funct Mater* 2018;**28**:1707440.
21. Shim G, Kim D, Kim J, Suh MS, Kim YK, Oh YK. Bacteriomimetic poly-γ-glutamic acid surface coating for hemocompatibility and safety of nanomaterials. *Nanotoxicology* 2017;**11**:762–70.
22. Kowalczuk M, Adamus G, Jedlinski Z. Synthesis of new graft polymers *via* anionic grafting of beta-butyrolactone on poly (methyl methacrylate). *Macromolecules* 1994;**27**:572–5.
23. Shim G, Choi HW, Lee S, Choi H, Yu YH, Park DE, et al. Enhanced intrapulmonary delivery of anticancer siRNA for lung cancer therapy using cationic ethylphosphocholine-based nanolipoplexes. *Mol Ther* 2013;**21**:816–24.
24. Akhila JS, Shyamjith D, Alwar M. Acute toxicity studies and determination of median lethal dose. *Curr Sci* 2007;**93**:917–20.
25. Kim MG, Shon Y, Kim J, Oh YK. Selective activation of anticancer chemotherapy by cancer-associated fibroblasts in the tumor microenvironment. *J Natl Cancer Inst* 2017;**109**:djw108.
26. Ahmad Z, Shah A, Siddiq M, Kraatz HB. Polymeric micelles as drug delivery vehicles. *RSC Adv* 2014;**4**:17028–38.
27. Wu Y, Yan M, Cui J, Yan Y, Li C. A multiple-functional Ag/SiO_2/organic based biomimetic nanocomposite membrane for high-stability protein recognition and cell adhesion/detachment. *Adv Funct Mater* 2015;**25**:5823–32.
28. Li F, Du M, Zheng Q. Dopamine/silica nanoparticle assembled, microscale porous structure for versatile superamphiphobic coating. *ACS Nano* 2016;**10**:2910–21.
29. Zhou J, Xiong Q, Ma J, Ren J, Messersmith PB, Chen P, et al. Polydopamine-enabled approach toward tailored plasmonic nanogapped nanoparticles: from nanogap engineering to multifunctionality. *ACS Nano* 2016;**10**:11066–75.
30. Bang SH, Yu YM, Hwang IC, Park HJ. Formation of size-controlled nano carrier systems by self-assembly. *J Microencapsul* 2009;**26**:722–33.
31. Weaver BA. How Taxol/PTX kills cancer cells. *Mol Biol Cell* 2014;**25**:2677–81.
32. Liu J, Zheng X, Yan L, Zhou L, Tian G, Yin W, et al. Bismuth sulfide nanorods as a precision nanomedicine for *in vivo* multimodal imaging-guided photothermal therapy of tumor. *ACS Nano* 2015;**9**:696–707.
33. Wang R, Zhao N, Xu FJ. Hollow nanostars with photothermal gold caps and their controlled surface functionalization for complementary therapies. *Adv Funct Mater* 2017;**27**:1700256–66.
34. Yang T, Tang Y, Liu L, Lv X, Wang Q, Ke H, et al. Size-dependent Ag_2S nanodots for second near-infrared fluorescence/photoacoustics imaging and simultaneous photothermal therapy. *ACS Nano* 2017;**11**:1848–57.
35. Li KC, Chu HC, Lin Y, Tuan HY, Hu YC. PEGylated copper nanowires as a novel photothermal therapy agent. *ACS Appl Mater Interfaces* 2016;**8**:12082–90.
36. Bettinger CJ, Bruggeman JP, Misra A, Borenstein JT, Langer R. Biocompatibility of biodegradable semiconducting melanin films for nerve tissue engineering. *Biomaterials* 2009;**30**:3050–7.
37. Gelderblom H, Verweij J, Nooter K, Sparreboom A. Cremophor EL: the drawbacks and advantages of vehicle selection for drug formulation. *Eur J Cancer* 2001;**37**:1590–8.
38. Utreja P, Jain S, Tiwary A. Evaluation of biosafety and intracellular uptake of Cremophor EL free paclitaxel elastic liposomal formulation. *Drug Deliv* 2012;**19**:11–20.
39. Imtiaz F, Shafique K, Mirza SS, Ayoob Z, Vart P, Rao S. Neutrophil lymphocyte ratio as a measure of systemic inflammation in prevalent chronic diseases in Asian population. *Int Arch Med* 2012;**5**:2.
40. Lattanzi S, Cagnetti C, Provinciali L, Silvestrini M. Neutrophil-to-lymphocyte ratio predicts the outcome of acute intracerebral hemorrhage. *Stroke* 2016;**47**:1654–7.
41. Hickman DL. Evaluation of the neutrophil: lymphocyte ratio as an indicator of chronic distress in the laboratory mouse. *Lab Anim* 2017;**46**:303–7.
42. Grigorian A, O'Brien CB. Hepatotoxicity secondary to chemotherapy. *J Clin Transl Hepatol* 2014;**2**:95–102.
43. Bonventre JV, Vaidya VS, Schmouder R, Feig P, Dieterle F. Next-generation biomarkers for detecting kidney toxicity. *Nat Biotechnol* 2010;**28**:436–40.